

Explainable Graph-theoretical Machine Learning: with Application to Alzheimer’s Disease Prediction

Narmina Baghirova^{1,2†}, Duy-Thanh Vũ^{2,3}, Duy-Cat Can^{2,3}, Christelle Schneuwly Diaz^{2,3},
Julien Bodlet^{2,3}, Guillaume Blanc², Georgi Hrusanov^{2,3}, Bernard Ries¹, and Oliver Y. Chén^{2,3‡},
for the Alzheimer’s Disease Neuroimaging Initiative*

¹Department of Informatics, University of Fribourg, Fribourg, Switzerland

²Platform of Bioinformatics, Lausanne University Hospital (CHUV), Lausanne, Switzerland

³Faculty of Biology and Medicine, University of Lausanne, Lausanne, Switzerland

[†]narmina.baghirova@unifr.ch; [‡]olivery.chen@chuv.ch.

Abstract

Alzheimer’s disease (AD) affects 50 million people worldwide and is projected to overwhelm 152 million by 2050. AD is characterized by cognitive decline due partly to disruptions in metabolic brain connectivity. Thus, early detection and accurate assessment of metabolic brain network impairments are crucial for AD management. Chief to identifying such metabolic impairments is the analysis of FDG-PET data. Despite advancements in graph-based approaches for different neuroimaging modalities, most studies using FDG-PET data rely on group-level analysis or thresholding. Group-level analysis can mask individual differences, while thresholding may overlook weaker yet biologically critical brain connections. Additionally, machine learning-based AD prediction largely focuses on univariate outcomes, such as disease status. Here, integrating insights from graph theory, machine learning, and biology, we introduce *explainable graph-theoretical machine learning* (XGML), a framework that: (a) employs kernel density estimation and dynamic time warping to construct individual metabolic brain graphs that capture the distance between pair-wise brain regions, and (b) identifies subgraphs most predictive of multivariate disease-related outcomes. To illustrate its efficacy, we apply XGML to construct metabolic brain graphs using FDG-PET scans from the Alzheimer’s Disease Neuroimaging Initiative and uncover subgraphs predictive of eight AD-related cognitive scores in previously unseen subjects. Overall, XGML demonstrates robust performance, particularly for predicting scores measuring learning, memory, language, praxis, and orientation, such as CDRSB ($r = 0.74$), ADAS11 ($r = 0.73$), and ADAS13 ($r = 0.71$). Moreover, XGML unveils key brain connections that are jointly but differentially predictive of several AD-related outcomes; they may serve as potential network biomarkers for assessing overall cognitive decline. Taken together, we demonstrate the promise of graph-theoretical machine learning in biomarker discovery and disease prediction and its potential to improve our understanding of network neural mechanisms underlying AD.

Keywords: Machine Learning, Graph Theory, Alzheimer’s disease, Network Biomarker, Disease prediction

*Data used in the preparation of this article are from the Alzheimer’s Disease Neuroimaging Initiative (ADNI) database (<http://adni.loni.usc.edu>). As such, the investigators within the ADNI contributed to the design and implementation of ADNI and/or provided data but did not participate in the analysis or writing of this paper. A complete list of ADNI investigators is available at: http://adni.loni.usc.edu/wp-content/uploads/how_to_apply/ADNI_Acknowledgement_List.pdf.

1 Introduction

Alzheimer’s disease (AD) is the predominant form of dementia [45]. It affects millions of individuals worldwide and leads to significant and growing global challenges [1]. As the disease progresses, it impairs memory, cognition and daily functioning, which, consequently, impacts patients’ quality of life and, eventually, results in death. Thus, it places a great deal of burden on caregivers and healthcare systems [16]. The limitations of current therapies [31], coupled with the fact that available treatments for AD are most effective in the early or middle stages [2], highlight the critical need for early detection and accurate assessment of the disease severity and its progression.

Central to evaluating the disease severity and cognitive impairment in AD are cognitive assessments [26]. Cognitive scores used during the assessment are quantifiable indicators of cognitive function impairment. Administering cognitive assessments, however, comes with several challenges. For example, the evaluations can be influenced by subjective factors such as an individual education level, cultural background, testing environment, and psychological states [32]. These limitations suggest the need for objective, standardized methods to assess patients’ cognitive status. Biomarkers, indicators of pathological and physical processes, emerge as a promising alternative [13]. While biomarkers such as cerebrospinal fluid tau and amyloid-beta offer valuable molecular and pathological insights into AD [20], they are nevertheless invasive. An important non-invasive alternative is neuroimaging data. In particular, Positron Emission Tomography (FDG-PET) offers insights into functional changes in the brain as AD progresses. Specifically, FDG-PET measures cerebral glucose metabolism which is tightly related to neuronal activity [3], enabling the detection of functional impairments that may appear before MRI-detectable atrophy [28]. Additionally, FDG-PET mirrors cognitive performance [18] making FDG-PET data particularly valuable for AD assessment. Indeed, prior work highlights FDG-PET as a powerful tool for cognitive assessment [11, 38].

While machine learning frameworks have been widely used to perform AD predictions, the existing methods tend to focus on predicting univariate outcomes, such as disease status [30, 39] and single AD-related measures, for example, that of univariate cognitive score [8, 24]. In parallel, network neuroscience, which applies graph theory to investigate brain networks, has gained important strides thanks to the increasing availability of neuroimaging data [5]. Recently, it has helped reveal structural changes in the brain [22], identify network biomarkers [15], and make advancements in disease prediction methods [44] in AD research. A common way to build brain graphs using neuroimaging data is to use vertices to represent brain regions of interest (ROIs) and edges to capture the relationships between the ROIs. The resulting graphs can be unweighted, often through thresholding techniques, or weighted, where statistical metrics are used to assign weights to the edges, where the weights reflect connectivity strengths. As discussed in Section 4, graph-based studies on FDG-PET data commonly involves using group-level analysis [19] and thresholding techniques; examples of such studies include [17, 34]. Use of group-level analysis can mask individual differences [29], while thresholding may overlook weaker yet biologically critical brain connections, thresholding may discard weaker yet biologically relevant edges, as disruptions between brain regions in AD are not yet fully understood [6].

To address these issues, in this study, we introduce *explainable graph-theoretical machine learning* (XGML). In brief, XGML constructs individual metabolic brain graphs that capture the distance between pair-wise brain regions using kernel density estimation and dynamic time warping. It then identifies subgraphs most predictive of multivariate disease-related outcomes using machine learning. To demonstrate its efficacy, we utilize data from the Alzheimer’s Disease Neuroimaging Initiative (ADNI) to construct metabolic distance graphs for each subject. The resulting distances enter a machine learning model, specifically, a Kernel Support Vector Regressor, to predict AD-related outcomes. Finally, using Permutation Feature Importance, XGML identifies key brain connections that are jointly but differentially predictive of eight AD-related outcomes. Although this study focuses on FDG-PET

data, we note that XGML can also be applied to other neuroimaging modalities, such as structural MRI, functional MRI, and amyloid-PET, for constructing brain distance graphs and identifying subgraphs most predictive of multivariate disease-related outcomes using machine learning.

Our main contributions are as follows. (1) We introduce a new, explainable approach to encode subject-specific FDG-PET data and, via machine learning, predict multivariate disease outcomes. (2) The XGML predicts eight AD-related cognitive scores, with correlations between the observed and predicted scores ranging from 0.41 to 0.74, with the highest values observed for CDRSB ($r = 0.74$), ADAS11 ($r = 0.73$), and ADAS13 ($r = 0.71$). (3) The top brain connections identified using XGML are neurobiologically relevant. Furthermore, although the top connections predictive of outcomes vary from outcome to outcome, some play an important role in predicting several outcomes. (4) Our results suggest the utility of graph-theoretical machine learning in AD prediction. The identified subgraphs may serve as potential network biomarkers for assessing cognitive decline in AD. (5) Finally, to promote transparency and reproducibility, we make the codes for constructing the graphs, making predictions, and selecting the top predictive edges available at: <https://anonymous.4open.science/r/XGML-2C2A>.

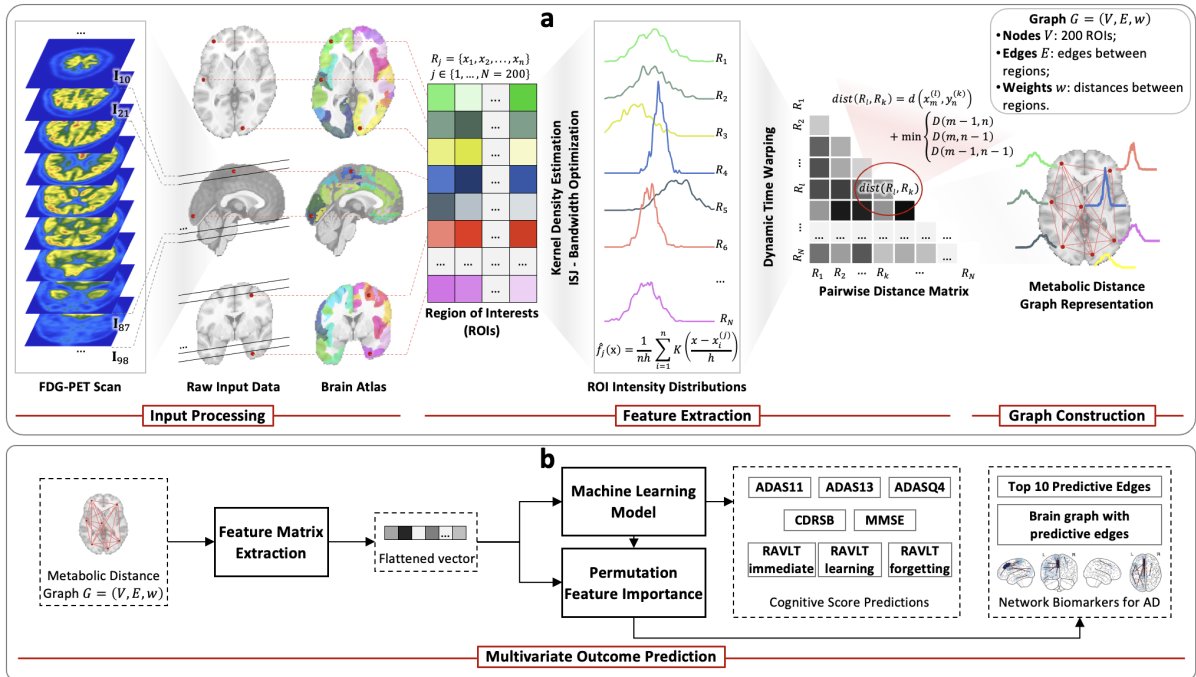


Figure 1: **A schematic representation of the explainable graph-theoretical machine learning (XGML) framework.** (a) The construction of metabolic distance graphs. (b) From high-dimensional brain graphs to multivariate outcome prediction.

2 Materials and Methods

Subjects. Data used in the preparation of this article are from the Alzheimer’s Disease Neuroimaging Initiative (ADNI) (adni.loni.usc.edu). The ADNI was launched in 2003 as a public-private partnership, led by Principal Investigator Michael W. Weiner, MD. The original goal of ADNI was to test whether serial magnetic resonance imaging (MRI), positron emission tomography (PET), other biological markers, and clinical and neuropsychological assessment can be combined to measure the progression of mild cognitive impairment (MCI) and early Alzheimer’s disease (AD). The current goals include validating biomarkers for clinical trials, improving the generalizability of ADNI data by increasing diversity in the

participant cohort, and to provide data concerning the diagnosis and progression of Alzheimer’s disease to the scientific community. For up-to-date information, see <https://adni.loni.usc.edu/>. More specifically, we consider two subsets of the ADNI database. The first subset, which we call Group I, will be used to construct individual metabolic distance graphs. The second subset, which we call Group II, will be used for network biomarker discovery and out-of-sample multivariate outcome prediction.

Specifically, Group I consists of 331 subjects, comprising 121 CN, 100 MCI, and 110 AD subjects. See Table 1 for details. Group II consists of 166 subjects, including 61 CN, 60 MCI, and 45 AD subjects. The eligibility criteria for Group II were the availability of both FDG-PET scans and cognitive scores. Only subjects with at least one FDG-PET scan and cognitive evaluation for all eight scores within a six-month window were included. For each subject, if more than one FDG-PET scan was available, we selected the scan with the date closest to the cognitive assessment. See Table 2 for details.

Table 1: Demographic characteristics of Group I. *No.* = Number of subjects. *Age* = Mean age (\pm standard deviation).

	CN		MCI		AD	
	No.	Age	No.	Age	No.	Age
Male	66	74.62 \pm 5.60	67	76.39 \pm 6.70	68	75.47 \pm 7.90
Female	55	74.71 \pm 5.33	33	72.25 \pm 7.54	42	72.61 \pm 7.53
Total	121	74.66 \pm 5.46	100	75.03 \pm 7.23	110	74.37 \pm 7.85

Table 2: Demographic characteristics of Group II. *No.* = Number of subjects. *Age* = Mean age (\pm standard deviation).

	CN		MCI		AD	
	No.	Age	No.	Age	No.	Age
Male	34	75.33 \pm 6.80	34	72.12 \pm 7.01	27	74.48 \pm 5.75
Female	27	74.24 \pm 6.62	26	73.41 \pm 9.11	18	72.29 \pm 6.37
Total	61	74.85 \pm 6.69	60	72.68 \pm 7.94	45	73.61 \pm 6.03

Cognitive scores. We consider eight cognitive and behavioural scores from five AD examinations. We chose these outcomes, in part, because they are from standard AD examinations that quantify the functioning and dysfunction of various cognitive aspects of the disease, and, in part, because we want to consider a real-world prediction scenario where some of the outcomes may be significantly correlated while others are not and to assess the performance of our method in dealing with general cases. These scores are: Clinical Dementia Rating Sum of Boxes (CDRSB) [41], 11- and 13-item versions of the Alzheimer’s Disease Assessment Scale-Cognitive Subscale (ADAS11 and ADAS13) and ADAS Delayed word recall (ADASQ4) [23], Mini-Mental State Examination (MMSE) [4], and three Rey Auditory Verbal Learning Test (RAVLT) [9] scores (immediate recall, learning, and percent forgetting). Specifically, CDRSB quantifies impairments across six domains: memory, orientation, judgment and problem-solving, community affairs, home and hobbies, and personal care. ADAS11 measures AD-related deficits such as memory, language, and praxis through tasks such as word recall and object naming, while ADAS13 expands on ADAS11 by including other tests for a more detailed assessment of memory and executive function. ADAS Delayed Word Recall (ADASQ4) assesses a patient’s episodic memory. The MMSE screens for cognitive impairment by assessing concentration,

attention, language and visuospatial skills. The RAVLT scores measure different aspects of memory: RAVLT_immediate evaluates episodic memory and learning, RAVLT_learning quantifies learning efficiency, and RAVLT_perc_forgetting evaluates delayed memory performance by evaluating how much information a person fails to retain after some period.

Image preprocessing. We utilize FDG-PET images from the ADNI dataset. For image preprocessing, we employed the standard CAT12 toolbox template, with a dimension of $113 \times 137 \times 113$ with isotropic voxel sizes of $1.5 \times 1.5 \times 1.5 \text{ mm}^3$, to ensure spatial alignment. Subsequently, we map each FDG-PET scan onto the Schaefer 2018 [35] brain atlas with 200 regions of interest (see Figure 1a). This allows us to identify the voxel-level glucose intensity values associated with each ROI.

An explainable way to encode subject-specific FDG-PET data. Now, we define distance graphs. First, to capture the underlying distribution of voxel intensities in each ROI, we employ Kernel Density Estimation (KDE). More specifically, let $R_j = \{x_1^{(j)}, x_2^{(j)}, \dots, x_n^{(j)}\}$ be the set of FDG-PET voxel intensity values for a given ROI R_j , for $j \in \{1, \dots, 200\}$, assumed to be drawn from an unknown distribution with an underlying density $f_j(x)$. We model this density via KDE, where the estimated probability density function $\hat{f}_j(x)$, corresponding to ROI R_j , is defined as:

$$\hat{f}_j(x) = \frac{1}{nh} \sum_{i=1}^n K\left(\frac{x - x_i^{(j)}}{h}\right),$$

where $K(\cdot)$ is a kernel function satisfying $\int_{-\infty}^{+\infty} K(u) du = 1$, $h > 0$ is the bandwidth controlling the smoothness of the estimate, and $x_i^{(j)}$ are the observed voxel intensity values in the corresponding brain region R_j . For further details on the KDE method, we refer our readers to [43]. When the sample size is large, the choice of the bandwidth parameter becomes critical, whereas the selection of the kernel function is comparatively less significant [25]. Thus, when identifying the underlying distribution in each ROI, we perform bandwidth tuning based on the Improved Sheather-Jones (ISJ) method, which determines an optimal bandwidth for the data [36]. By applying KDE to each brain region, we obtain probability density functions (PDFs) for each brain region.

We then quantify the distances between the PDFs using Dynamic Time Warping (DTW). Although DTW is traditionally used to align and compare temporal sequences of varying lengths or speeds, we treat each PDF as a discrete sequence; this allows us to apply DTW directly to the PDFs. More specifically, let $R_k = (x_1^{(k)}, x_2^{(k)}, \dots, x_n^{(k)})$ and $R_\ell = (y_1^{(\ell)}, y_2^{(\ell)}, \dots, y_m^{(\ell)})$, for $k, \ell \in \{1, \dots, 200\}$, denote two discrete representations of PDFs corresponding to ROIs R_k and R_ℓ , of length n and m , respectively. Then, we construct an $n \times m$ cost matrix D , where $D(i, j)$ accumulates the minimal alignment cost up to indices i and j . The recursive definition is as follows:

$$D(i, j) = d(x_i^{(k)}, y_j^{(\ell)}) + \min \begin{cases} D(i-1, j), \\ D(i, j-1), \\ D(i-1, j-1), \end{cases}$$

where $d(x_i^{(k)}, y_j^{(\ell)})$ denotes a distance measure between the values $x_i^{(k)}$ and $y_j^{(\ell)}$, $D(0, 0) = 0$ is the base case, and $D(i, 0) = D(0, j) = \infty$, for $i > 0$ or $j > 0$. The final value $D(n, m)$ is the distance value between region R_k and R_ℓ , which we denote by $\text{dist}(R_k, R_\ell)$. Note that the final distance value cannot be negative because the recursive process only adds non-negative distance measures starting from a base case zero. For more details on the DTW method, we refer our readers to [33].

Finally, we construct the *distance graph*, which is an undirected, weighted graph $G = (V, E, w)$, as follows:

- V is the set of vertices, corresponding to the 200 ROIs.

- E is the set of edges, including all possible edges between any two pairs of vertices.
- $w : E \rightarrow \mathbb{R}^+$ is a weight function assigning a positive real number to each edge. More specifically, the weight of an edge $uv \in E$ is given by $\text{dist}(u, v)$.

Graph-theoretical machine learning. Here we define the XGML framework, consisting of three key steps: (1) constructing individual metabolic distance graphs as described above, (2) using edge weights as input features in a predictive modeling (e.g., kernel support vector regressor) setting, and (3) identifying and explaining the most predictive subgraphs using permutation importance. See Figure 1 for an illustration of the framework.

Within the framework, each distance graph is represented by a 200×200 weighted adjacency matrix, where rows and columns correspond to the 200 ROIs, denoted by R_1, \dots, R_{200} . Each entry (i, j) is defined as $\text{dist}(R_i, R_j)$, for $i \neq j$, and $\text{dist}(R_i, R_j) = 0$, for $i = j$, for $i, j \in \{1, \dots, 200\}$. We transform this matrix into a feature vector by extracting and flattening the upper triangular elements (excluding the diagonal), thereby capturing distances between any pair of brain regions. This feature vector then serves as input to a machine learning model that maps high-dimensional features onto multivariate outcomes. More concretely, we employ a Kernel Support Vector Regressor (Kernel SVR) in a MultiOutputRegressor framework, with high-dimensional network features as inputs and multivariate cognitive scores as outcomes. We perform hyperparameter tuning using a five-fold cross-validation, and evaluate the model with the optimal hyperparameters via a leave-one-out cross-validation (LOOCV). We assess the model’s performance by computing the correlation coefficient (r) between the observed and predicted scores for each outcome.

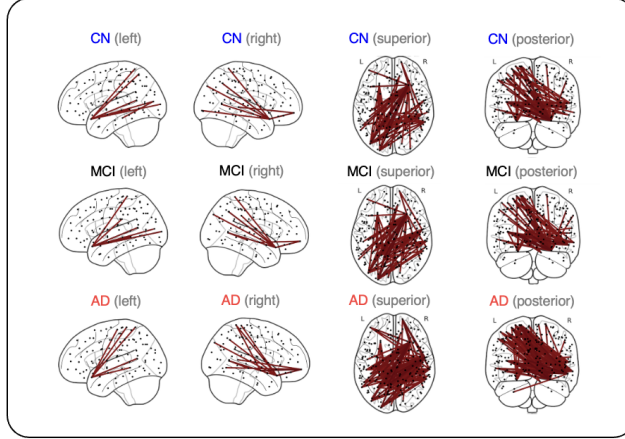
To interpret the contribution every edge makes to the prediction of each cognitive score, we conduct a permutation importance analysis. Specifically, we randomly shuffle the feature value of a corresponding edge while leaving values of all other edges intact; we then measure the drop in predictive performance due to the change of this edge. Finally, we select the ten edges, whose values, when shuffled, give rise to a significant decrease in prediction performance: these edges are most relevant to the prediction of the corresponding outcome.

3 Results

After applying the XGML framework to FDG-PET scans from the ADNI dataset to predict eight AD-related cognitive scores, as detailed at the beginning of Section 2, here we present the results.

Overall distance values analysis. To analyze metabolic distance variations across CN, MCI, and AD subjects, we first constructed group-level metabolic distance graphs using subjects from Group I. We applied a trimmed mean to individual distance matrices for each subject within each group to reduce outlier effects. Subsequently, we normalized the resulting matrices to a 0–1 range using min-max normalization. Furthermore, we assessed the average distance values (across all edges) among three groups; our results suggest that the average metabolic distance increases from CN individuals (0.3581), to MCI subjects (0.3767), and to AD patients (0.3938). Subsequently, we examined, in addition to increasing average network strength values, whether the prevalence of prominent distance edges (i.e., edges with large values) increases as the disease progresses. Specifically, we counted edges that exceed thresholds of 0.70, 0.75, and 0.80 for the CN and AD groups. Using a threshold of 0.70, the CN group has 520 high-valued edges, the MCI group has 438, and the AD group has 748. Using a threshold of 0.75, the CN group has 272 high-valued edges, MCI has 260, and the AD group has 370. Using a threshold of 0.80, the CN group has 132 high-valued edges, MCI has 132, and the AD group has 214. Figure 2a illustrates the high-valued distance edges; we present edges with distance values exceeding 0.80 for illustration purposes.

a Metabolic distance graphs in **CN** (cognitively normal), **MCI** (mild cognitive impaired), and **AD** subjects



b Metabolic distance graphs predict multivariate AD-related outcomes in new subjects

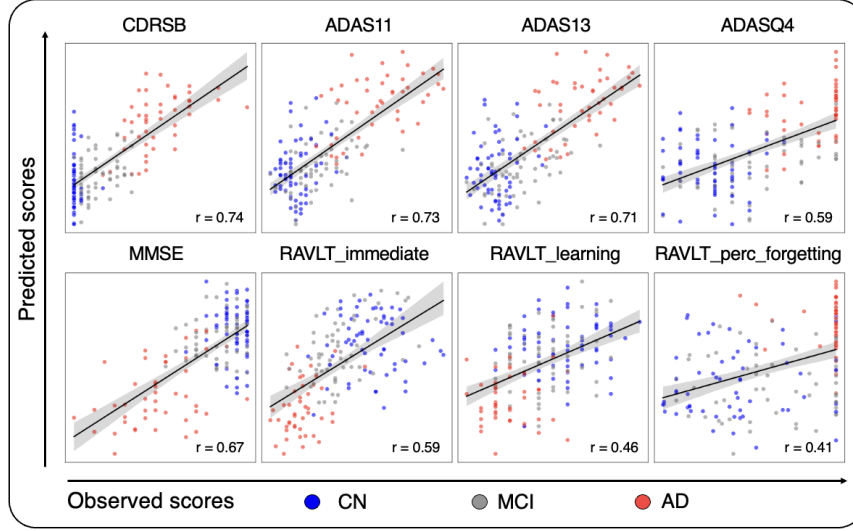


Figure 2: Inter- and intra-group metabolic brain network differences and their prediction of individual multivariate AD-related cognitive scores. (a) Metabolic distance graphs derived from FDG-PET scans corresponding to CN, MCI and AD groups. Each graph is shown from four viewpoints (left, right, superior, and posterior), overlaid with edges whose distance values are above 0.80. (b) Out-of-sample prediction performance of XGML for predicting eight cognitive scores. The x- and y-axis represent observed and predicted values, respectively. Each line indicates goodness-of-fit; each shaded area represents the 95% confidence bands; the accuracy is quantified using the Pearson correlation coefficient (in the bottom right of each panel).

Predictive performance. Next, we present the model's performance on predicting eight AD-related cognitive outcomes leveraging the defined distance graphs. We performed out-of-sample predictions using data from Group II subjects to evaluate the reproducibility and generalizability of the model. Our results suggest that XGML achieved prediction accuracy ranging from 0.41 to 0.74 for the eight outcomes with an average correlation of $r = 0.61$ across eight predictions. In particular, the model obtained the highest accuracies for CDRSB ($r = 0.74$), ADAS11 ($r = 0.73$), and ADAS13 ($r = 0.71$). See Figure 2b for details.

The top ten predictive network features and their neurological implications. To investigate the network features' contribution to the prediction and their neurobiological relevance, we used XGML to extract subgraphs most predictive of each cognitive score, consisting of the top ten predictive edges and their endpoints, and uncover their anatomical locations (see Figure 3). To quantify each brain region's contribution to predicting a cognitive score, we computed the sum of the outgoing edges from that region and then normalized these values. Regions that serve as endpoints for a larger number of the top ten predictive edges are more relevant for predicting the respective cognitive scores.

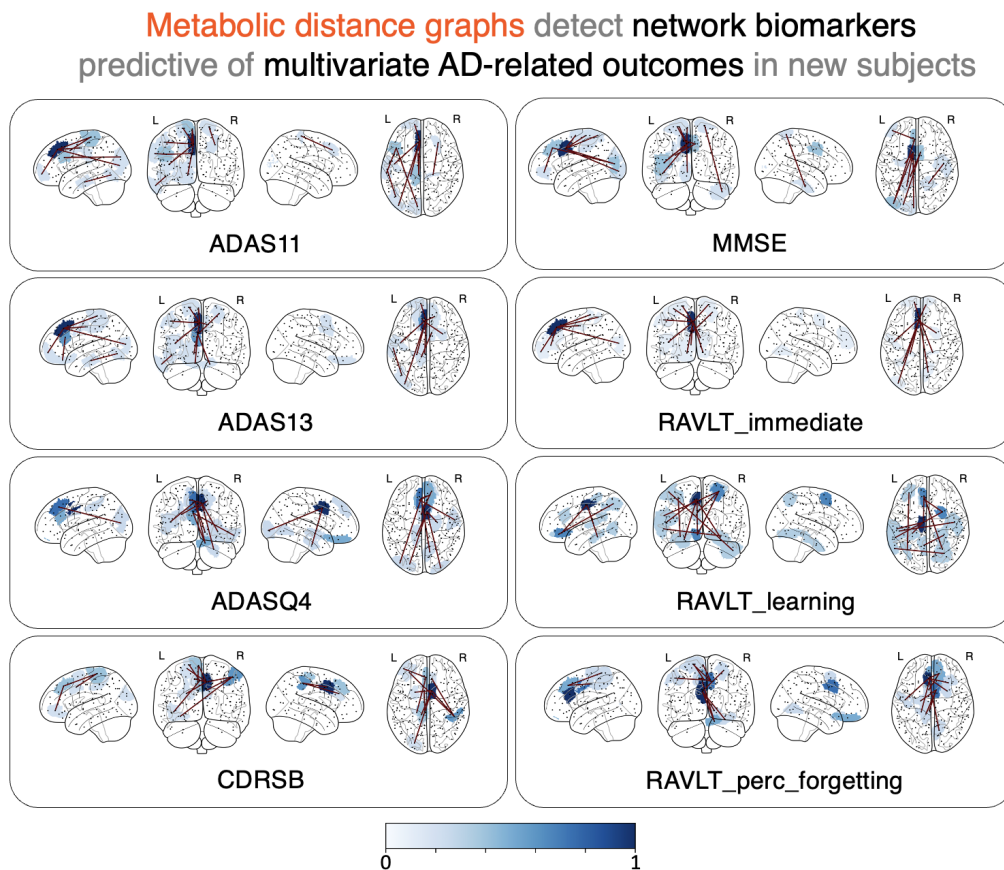


Figure 3: **The top 10 most predictive edges for each cognitive score.** Each box corresponds to a cognitive score and shows the most important edges, from four views: left, posterior, right, and superior, for predicting that score. The color gradient of brain regions reflects their predictive importance, with darker blue indicating higher relevance.

The most predictive regions for ADAS11, ADAS13, and ADASQ4 scores, measures of memory, language, and praxis, are located in the frontal, parietal, and temporal lobes. Noticeably, the key regions for ADAS11 and ADAS13 are predominantly in the left hemisphere. This is consistent with the functions of these regions: the temporal, frontal, and parietal lobes support memory-related functions, the left temporal and frontal lobes are mainly responsible for language-related functions, and the parietal lobe is critical for praxis. The most important regions for CDRSB, a measure of orientation, judgment and problem-solving, community affairs, home and hobbies, and personal care, mainly span the frontal and parietal lobes. This aligns with the function of these regions: orientation mainly relies on parietal and frontal areas; judgment and problem-solving, and daily activities are primarily linked to the frontal lobes, with the parietal region supporting sensory integration. For MMSE, a measure of concentration, attention, memory, naming, and visuospatial skills, XGML identifies the most predictive regions in the left frontal, temporal, parietal, and occipital lobes. This is in line with

Circular plots for the **eight cognitive scores** showing the distribution of the **top 10 most predictive edges** across the **Yeo 7 networks**

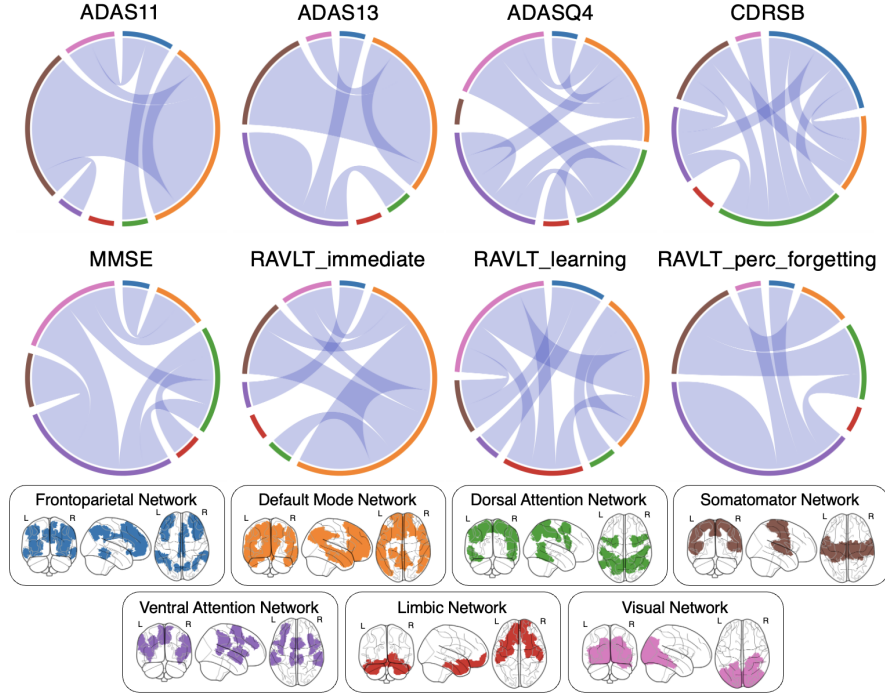


Figure 4: **The functional distribution of the top ten most predictive edges for each of the eight cognitive scores.** Each plot is color-coded to match the seven Yeo networks shown in the boxes below.

the known functions of these regions, with the occipital lobe contributing to visuospatial processing. Lastly, RAVLT scores measure distinct memory-related functions: RAVLT_immediate evaluates episodic memory, RAVLT_perc_forgetting delayed memory, and RAVLT_learning learning efficiency. The key regions identified by XGML are in the frontal, parietal, and temporal lobes; this aligns with the fact that memory processing relies partly on the temporal lobe for encoding and retrieval with support from the frontal lobe for processing and the parietal cortex for retrieval. See [14, 21] for a reference on the functions of the brain areas discussed herein.

Next, we investigated how the top ten predictive edges for each cognitive score are functionally distributed in the brain. To do so, we mapped the key edges onto the Yeo 7 functional networks [46]. Our results suggest that for ADAS11 and ADAS13, the top ten predictive edges predominantly have endpoints in the Default Mode Network (implicated in self-referential thought and memory retrieval) [7] and Somatomotor network (plays a role in preparing and coordinating motor actions) [10]; the edges predictive of ADAS13, in addition, have endpoints in Ventral Attention network (responsible for mediating stimulus-driven reorienting of attention) [42]. Meanwhile, for ADASQ4, the predictive edges span the Ventral Attention, the Default Mode, Dorsal Attention network (responsible for top-down, voluntary allocation of attention to locations or features in space) [42], and Visual network (responsible for processing information about static and moving objects) [37]. The top ten predictive edges for CDRSB mainly involve the Dorsal Attention and Frontoparietal network (supports working memory and higher-order cognitive control) [27]. The predictive edges for MMSE mainly have endpoints in the Ventral Attention, Visual, and Dorsal Attention networks. Finally, regarding the RAVLT measures, the edges for RAVLT_immediate have endpoints mainly in the Default Mode, those for RAVLT_learning have endpoints mainly in the Default Mode and Visual networks, and edges for RAVLT_perc_forgetting span the Ventral Attention and Somatomotor networks. See Figure 4 for details.

Average connectivity strength across the top ten most predictive edges for each cognitive score, comparing CN and AD subjects

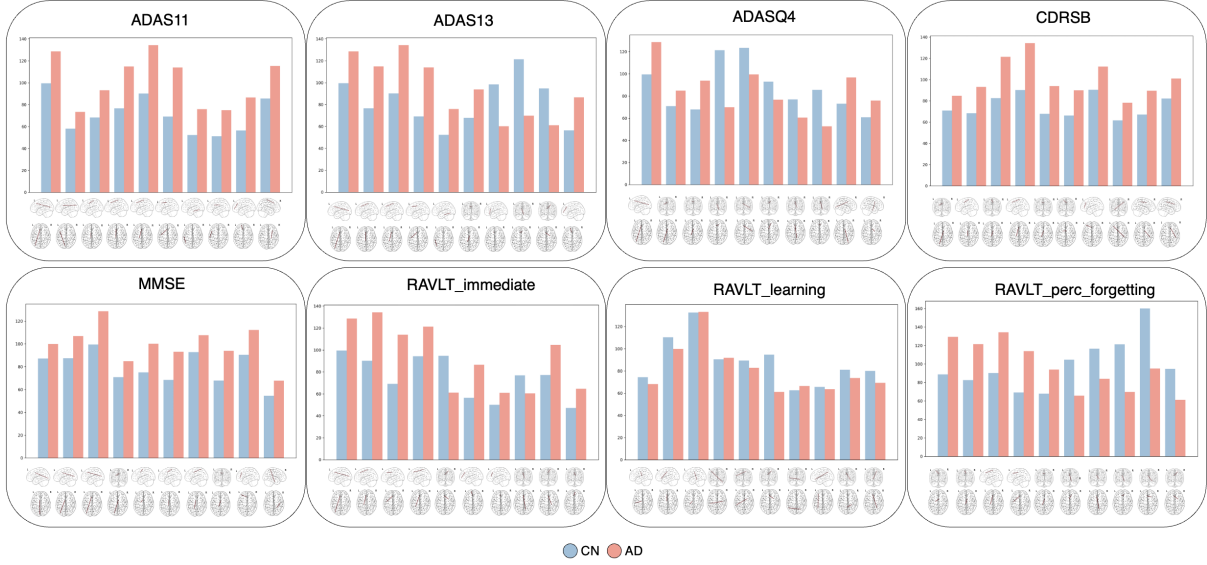


Figure 5: **The average distance value of the top ten most predictive edges between CN (blue) and AD (red) groups.** Each bar within a box corresponds to one of the top ten most predicting edges of the corresponding cognitive score. In general, the distance value is higher, across different edges and different cognitive scores, for the AD patients compared to CN subjects.

Furthermore, we probed into the average distance value difference between CN and AD groups for the top ten most predictive edges for each cognitive score (see Figure 5). Our findings suggest that each cognitive score has unique metabolic network underpinnings; the varying distance values - of even the same edge - associated with different cognitive scores, therefore, not only give rise to, but are potentially a chief reason why they are predictive of the eight cognitive scores. More specifically, for the scores assessing broader or more complex cognitive functions, such as ADAS11, ADAS13, CDRSB, and MMSE, AD patients mainly exhibit higher distances on these top predictive edges. While for memory-specific measures, such as ADASQ4, RAVLT_learning, and RAVLT_perc_forgetting, CN subjects often show higher distances on the top ten most predictive edges.

Finally, we further investigated if there are top predictive features associated with and predictive of several cognitive scores. Our results show that, although no single edge was predictive of all eight scores, several edges were repeatedly identified as top predictors for up to four or five scores, as shown on Figure 6. This hints that there potentially exist a complex hierarchy of metabolic networks, where some edges are specially involved in one cognitive score/domain, and others may be associated with several cognitive scores/domains.

4 Discussions and Conclusion

In this paper, we introduced explainable graph-theoretical machine learning (XGLM), a framework that combines insights from graph theory, machine learning, and biology. To demonstrate its efficacy, we constructed individual metabolic distance brain graphs using FDG-PET neuroimaging from the ADNI dataset and used their edge weights as network features to predict multivariate AD-related outcomes.

There are a few methodological contributions of the paper. First, we introduce a new approach for constructing individual metabolic brain graphs from FDG-PET data that is explainable. Particularly, such an approach enables the construction of subjective-specific graphs, rather than relying on

Edges in **metabolic distance graphs** which serve as top ten most predictive edges across several AD-related outcomes

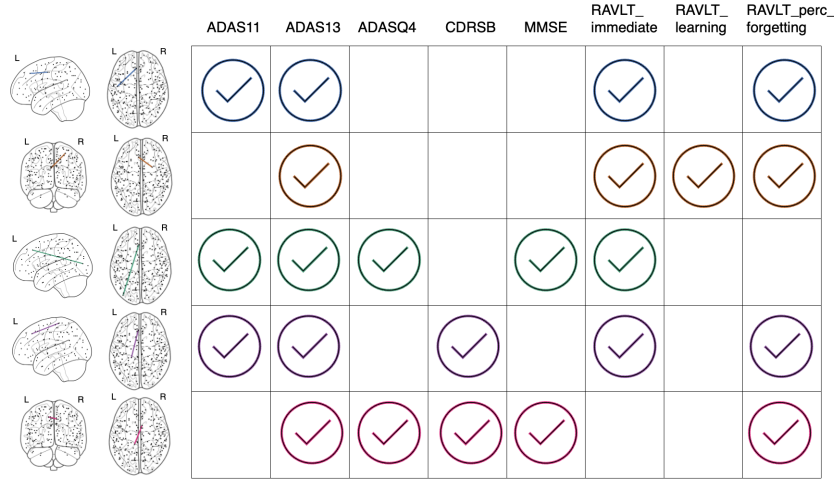


Figure 6: **The projection from top predictive edges to several cognitive outcomes.** Each row corresponds to one of the frequently occurring edges, and each column represents a specific cognitive score. A check mark indicates that the given edge was among the top ten most predictive for that particular score. This illustrates certain edges are associated with multiple cognitive domains.

group-level analysis. Additionally, since the disruptions between brain regions in AD are not yet fully understood, we use all edge weights in our analysis instead of applying thresholds, thus avoiding pre-selecting connections, for example via thresholding, as done in previous studies. Second, compared to univariate prediction tasks (e.g., assessing AD status or severity) using network features, our framework can predict multivariate AD-related outcomes using brain graphs.

Graphs constructed from FDG-PET mainly rely on group-level analysis since each scan contains a single numerical value per voxel. When considering brain regions of interest (ROIs), the number of voxels per region varies, making standard statistical methods such as correlation, which require equal measures, impractical. To address this, a typical approach in the literature is to extract a summary statistic (e.g., the mean or median FDG uptake) for each ROI, reducing each region to a single value. Since correlations cannot be computed from a single value, they are calculated across patients, thereby masking subject-specific differences. In our study, to account for the varying number of voxels per region, we use KDE to find the PDFs associated with each ROI. Given that the number of voxels varies across ROIs, the resulting PDFs may differ in length. To account for this variability, we employ DTW, which calculates the distances between those PDFs and handles misalignments and shape differences among the distributions, even when they differ in size or exhibit non-linear shifts. Additionally, one can transform the distance into a similarity measure, for instance, by applying an exponential decay transformation as follows: $e^{-\text{dist}(R_k, R_\ell)}$. This would imply that higher distances correspond to lower similarity and vice versa. When we applied this transformation, it, however, led to lower prediction performance using the same machine learning model. We use 200 brain regions throughout the paper, but our framework can be generalized to different ROI counts. Finally, we note that while our study applied XGML to FDG-PET scans, the framework can also be applied to other neuroimaging modalities, such as structural MRI, functional MRI, and amyloid-PET, for constructing distance graphs and identifying predictive subgraphs using machine learning methods.

Neurobiologically, our findings not only support previous findings about brain connectivity disruptions as AD progresses [12] but also offer a few new neurobiological insights. Our results suggest that metabolic distance values are more strongly associated with and predictive of scores assessing complex cognitive functions, such as CDRSB, ADAS11, and ADAS13, than with those focused solely on memory

evaluation, such as the RAVLT measures and ADASQ4. In addition, the discovered key brain connections that significantly and differentially predict different cognitive scores highlights their potential as network biomarkers for assessing domain-specific cognitive decline. For instance, since CDRSB evaluates impairment in memory, orientation, judgment and problem-solving, community affairs, home and hobbies, and personal care, the key brain connections identified for this score could serve as potential network biomarkers for evaluating these domain-specific cognitive functions. Notably, the key brain regions identified as chief predictors of each cognitive score are located in brain regions whose functions align with the cognitive domains being assessed by the cognitive score. This not only strengthens the predictive potency of the edges but also their neurological relevance.

In parallel, we discovered brain edges whose strength is associated with several cognitive scores and may, therefore, potentially serve as network biomarkers for assessing general cognitive decline in AD. Interestingly, when comparing the connectivity strength of the top ten predictive edges between CN and AD patients, we found that some of the edges have decreased distance value in AD patients. Based on the cognitive domains assessed by the corresponding scores where this decrease occurred, we hypothesize that while AD broadly disrupts neural circuits supporting complex cognitive functions, language, and praxis, the neural circuits involved in memory processing may engage compensatory mechanisms.

Moreover, our results suggest that our framework effectively captures the progressive disruption of metabolic (dis)connectivity as AD progresses. For example, we show that there is an increased average metabolic distance in AD subjects compared to CN subjects. The observed increase suggests progressive disruptions in brain connectivity, aligning with earlier findings on connectivity disruptions in AD and supporting the concept of AD as a "disconnection syndrome" [12]. Our finding of the rising prevalence of high-distance edges in AD patients further indicates the idea that large-scale network alterations underlie cognitive decline.

There are a few limitations with our framework. First, we conducted the analysis using data from one study. Although we illustrated the generalizability of the model and the network biomarkers using cross-validations, their broad generalizability to external cohorts needs to be further tested. Second, we applied XGML to study brain network using FDG-PET scans. Future work needs to evaluate the efficacy of XGML applied to other neuroimaging modalities, such as structural MRI, functional MRI, or amyloid-PET. Third, XGML consists of several steps, each involving parameter choices that may influence the final performance. Although we conducted parameter tuning only where possible, a more thorough parameter search could potentially yield improved outcomes. Finally, although the average prediction accuracy ($r = 0.61$) is high, there is room for improvement. Incorporating additional data modalities may help improve the accuracy by providing more comprehensive, complimentary information of AD pathophysiology [40, 47]. For example, integrating multimodal neuroimaging, genetic, and proteomic network data may further improve the predictive performance.

To conclude, the search for explainable graph-theoretical machine learning to study brain networks predictive of multivariate outcomes is still in its infancy. We hope that our work may bring some new ideas to our colleagues about individual network biomarker discovery and disease prediction. We welcome our colleagues to apply and evaluate our approach in diverse datasets and settings to advance our knowledge about how the brain is wired, how its network disruptions and discrepancies give rise to brain diseases, and how to make use of insights about brain graphs for early and timely disease assessment, and, perhaps one day, better management and treatment.

5 Acknowledgments

N.B. and O.Y.C. conceptualized the study. N.B. developed the methods, wrote the codes, and conducted the analyses. N.B. obtained all the results. D.T.V. prepared and pre-processed the data. D.C.C plotted Figures 1 and 4 and N.B. plotted the rest of the figures. D.C.C. and C.S.D. reviewed portions of the code

and provided feedback on how to improve the figures. J.B., G.B., and G.H. provided machine learning support. B.R. provided guidance to N.B. N.B. and O.Y.C. wrote the manuscript, with comments from all other authors.

Data collection and sharing for the Alzheimer’s Disease Neuroimaging Initiative (ADNI) is funded by the National Institute on Aging (National Institutes of Health Grant U19AG024904). The grantee organization is the Northern California Institute for Research and Education. In the past, ADNI has also received funding from the National Institute of Biomedical Imaging and Bioengineering, the Canadian Institutes of Health Research, and private sector contributions through the Foundation for the National Institutes of Health (FNIH) including generous contributions from the following: AbbVie, Alzheimer’s Association; Alzheimer’s Drug Discovery Foundation; Araclon Biotech; BioClinica, Inc.; Biogen; BristolMyers Squibb Company; CereSpir, Inc.; Cogstate; Eisai Inc.; Elan Pharmaceuticals, Inc.; Eli Lilly and Company; EuroImmun; F. Hoffmann-La Roche Ltd and its affiliated company Genentech, Inc.; Fujirebio; GE Healthcare; IXICO Ltd.; Janssen Alzheimer Immunotherapy Research & Development, LLC.; Johnson & Johnson Pharmaceutical Research & Development LLC.; Lumosity; Lundbeck; Merck & Co., Inc.; Meso Scale Diagnostics, LLC.; NeuroRx Research; Neurotrack Technologies; Novartis Pharmaceuticals Corporation; Pfizer Inc.; Piramal Imaging; Servier; Takeda Pharmaceutical Company; and Transition Therapeutics.

Disclosure of Interests. The authors have no competing interests to declare that are relevant to the content of this article.

References

- [1] Worldwide dementia cases to triple by 2050. Alzheimer’s Research UK (2021), <https://www.alzheimersresearchuk.org/news/worldwide-dementia-cases-to-triple-by-2050/>
- [2] How alzheimer’s disease is treated. National Institute on Aging (2023), <https://www.nia.nih.gov/health/alzheimers-treatment/how-alzheimers-disease-treated>
- [3] Arbizu, J., Morbelli, S., Minoshima, S., et al.: Snmmi procedure standard/eanm practice guideline for brain [18f]fdg pet imaging, version 2.0. *Journal of Nuclear Medicine* (2024)
- [4] Arevalo-Rodriguez, I., Smailagic, N., Roqué I Figuls, M., et al.: Mini-mental state examination (mmse) for the detection of alzheimer’s disease and other dementias in people with mild cognitive impairment (mci). *Cochrane Database of Systematic Reviews* **3** (2015)
- [5] Bassett, D.S., Sporns, O.: Network neuroscience. *Nature Neuroscience* **20**, 353–364 (2017)
- [6] Brier, M., Thomas, J., Ances, B.: Network dysfunction in alzheimer’s disease: Refining the disconnection hypothesis. *Brain connectivity* **4**, 299–311 (2014)
- [7] Buckner, R.L., Andrews-Hanna, J.R., Schacter, D.L.: The brain’s default network: anatomy, function, and relevance to disease. *Annals of the New York Academy of Sciences* **1124**, 1–38 (2008)
- [8] Bueno-Cayo, A.M., del Rio Carmona, M., Castell-Enguix, R., et al.: Predicting scores on the mini-mental state examination (mmse) from spontaneous speech. *Behavioral Sciences* **12**(9), 339 (2022)
- [9] Carone, D.: E. strauss, e. m. s. sherman, & o. spreen, a compendium of neuropsychological tests: Administration, norms, and commentary. *Applied Neuropsychology* **14**, 62–63 (2007)
- [10] Chenji, S., Jha, S., Lee, D., Brown, M., Seres, P., Mah, D., Kalra, S.: Investigating default mode and sensorimotor network connectivity in amyotrophic lateral sclerosis. *PLOS ONE* **11**(6), 1–14 (2016)
- [11] Choi, H., Jin, K.H.: Predicting cognitive decline with deep learning of brain metabolism and amyloid imaging. *Behavioural Brain Research* **344**, 103–109 (2018)
- [12] Delbeuck, X., Van der Linden, M., Collette, F.: Alzheimer’s disease as a disconnection syndrome? *Neuropsychology Review* **13**(2), 79–92 (2003)
- [13] Dubois, B., von Arnim, C.A., Burnie, N., et al.: Biomarkers in alzheimer’s disease: role in early and differential diagnosis and recognition of atypical variants. *Alzheimer’s Research & Therapy* **15**, 175 (2023)
- [14] Gazzaniga, M.S., Ivry, R.B., Mangun, G.R.: *Cognitive Neuroscience: The Biology of the Mind*. W. W. Norton & Co Inc, 5th edn. (2018)
- [15] Gomez-Ramirez, J., Wu, J.: Network-based biomarkers in alzheimer’s disease: review and future directions. *Frontiers in Aging Neuroscience* **6**, 12 (2014)
- [16] Grabher, B.J.: Effects of alzheimer disease on patients and their family. *Journal of Nuclear Medicine Technology* **46**(4), 335–342 (2018)
- [17] Guo, J., Qiu, W., Li, X., et al.: Predicting alzheimer’s disease by hierarchical graph convolution from positron emission tomography imaging. In: 2019 IEEE International Conference on Big Data (Big Data). pp. 5359–5363 (2019)

- [18] Henkel, R., Brendel, M., Paolini, M., et al.: Fdg pet data is associated with cognitive performance in patients from a memory clinic. *Journal of Alzheimer's Disease* **78**(1), 207–216 (2020)
- [19] Huang, S.Y., Hsu, J.L., Lin, K.J., Hsiao, I.T.: A novel individual metabolic brain network for 18f-fdg pet imaging. *Frontiers in Neuroscience* **14** (2020)
- [20] Jangampalli Adi, P., Baig, J., Islam, M.A., et al.: Amyloid- β and phosphorylated tau are the key biomarkers and predictors of alzheimer's disease. *Aging and Disease* **16**(2), 658–682 (2024)
- [21] Jessell, T.M., Kandel, E.R., Siegelbaum, S.A.: *Principles of Neural Science*, Sixth Edition. McGraw-Hill Education / Medical (2021)
- [22] John, M., Ikuta, T., Ferbinteanu, J.: Graph analysis of structural brain networks in alzheimer's disease: beyond small world properties. *Brain Structure and Function* **222**, 923–942 (2017)
- [23] Kueper, J.K., Speechley, M., Montero-Odasso, M.: The alzheimer's disease assessment scale-cognitive subscale (adas-cog): Modifications and responsiveness in pre-dementia populations. a narrative review. *Journal of Alzheimer's Disease : JAD* **63**(2), 423–444 (2018)
- [24] Lin, Q., Rosenberg, M.D., Yoo, K., et al.: Resting-state functional connectivity predicts cognitive impairment related to alzheimer's disease. *Frontiers in Aging Neuroscience* **10**, 94 (2018)
- [25] Marron, J., Nolan, D.: Canonical kernels for density estimation. *Statistics & Probability Letters* **7**(3), 195–199 (1988)
- [26] McKhann, G.M., Knopman, D.S., Chertkow, H., et al.: The diagnosis of dementia due to alzheimer's disease: Recommendations from the national institute on aging-alzheimer's association workgroups on diagnostic guidelines for alzheimer's disease. *Alzheimer's & Dementia* **7**(3), 263–269 (2011)
- [27] Menon, V.: Large-scale brain networks and psychopathology: a unifying triple network model. *Trends in Cognitive Sciences* **15**(10), 483–506 (2011)
- [28] Mosconi, L., Sorbi, S., de Leon, M.J., et al.: Hypometabolism exceeds atrophy in presymptomatic early-onset familial alzheimer's disease. *Journal of Nuclear Medicine* **47**(11), 1778–1786 (2006)
- [29] Parasuraman, R., Jiang, Y.: Individual differences in cognition, affect, and performance: Behavioral, neuroimaging, and molecular genetic approaches. *NeuroImage* **59**(1), 70–82 (2012), *neuroergonomics: The human brain in action and at work*
- [30] Park, S.W., Yeo, N.Y., Lee, J., et al.: Machine learning application for classification of alzheimer's disease stages using ^{18}f -flortaucipir positron emission tomography. *BioMed Engineering OnLine* **22**, 40 (2023)
- [31] Passeri, E., Elkhoury, K., Morsink, M., et al.: Alzheimer's disease: Treatment strategies and their limitations. *International Journal of Molecular Sciences* **23**(22), 13954 (2022)
- [32] Rosselli, M., Uribe, I.V., Ahne, E., et al.: Culture, ethnicity, and level of education in alzheimer's disease. *Neurotherapeutics: The Journal of the American Society for Experimental NeuroTherapeutics* **19**(1), 26–54 (2022)
- [33] Sakoe, H.: Dynamic programming algorithm optimization for spoken word recognition. *IEEE Transactions on Acoustics, Speech, and Signal Processing* **26**, 159–165 (1978)

- [34] Sanabria-Diaz, G., Martínez-Montes, E., Melie-Garcia, L.: Glucose metabolism during resting state reveals abnormal brain networks organization in the alzheimer’s disease and mild cognitive impairment. *PLoS ONE* **8**(7), e68860 (2013)
- [35] Schaefer, A., Kong, R., Gordon, E.M., Laumann, T.O., Zuo, X.N., Holmes, A.J., Eickhoff, S.B., Yeo, B.T.T.: Local-global parcellation of the human cerebral cortex from intrinsic functional connectivity mri. *Cerebral Cortex* **28**(9), 3095–3114 (2018)
- [36] Sheather, S.J., Jones, M.C.: A reliable data-based bandwidth selection method for kernel density estimation. *Journal of the Royal Statistical Society. Series B (Methodological)* **53**(3), 683–690 (1991)
- [37] Shen, W., Tu, Y., Gollub, R.L., Ortiz, A., Napadow, V., Yu, S., Wilson, G., Park, J., Lang, C., Jung, M., Gerber, J., Mawla, I., Chan, S.T., Wasan, A.D., Edwards, R.R., Kaptchuk, T., Li, S., Rosen, B., Kong, J.: Visual network alterations in brain functional connectivity in chronic low back pain: A resting state functional connectivity and machine learning study. *NeuroImage: Clinical* **22**, 101775 (2019)
- [38] Shokouhi, S., Claassen, D., Kang, H., et al.: Longitudinal progression of cognitive decline correlates with changes in the spatial pattern of brain ¹⁸f-fdg pet. *Journal of Nuclear Medicine* **54**(9), 1564–1569 (2013)
- [39] Sorour, S.E., El-Mageed, A.A.A., Albarrak, K.M., et al.: Classification of alzheimer’s disease using mri data based on deep learning techniques. *Journal of King Saud University - Computer and Information Sciences* **36**(2), 101940 (2024)
- [40] Thanh, V.D., LE, T.T., Tuan, P.M., et al.: Tensor kernel learning for classification of alzheimer’s conditions using multimodal data. *bioRxiv* (2024)
- [41] Tzeng, R.C., Yang, Y.W., Hsu, K.C., et al.: Sum of boxes of the clinical dementia rating scale highly predicts conversion or reversion in predementia stages. *Frontiers in Aging Neuroscience* **14**, 1021792 (2022)
- [42] Vossel, S., Geng, J.J., Fink, G.R.: Dorsal and ventral attention systems: Distinct neural circuits but collaborative roles. *The Neuroscientist* **20**(2), 150–159 (2014)
- [43] Weglarczyk, S.: Kernel density estimation and its application. *ITM Web of Conferences* **23**, 1–8 (2018)
- [44] Wei, R., Li, C., Fogelson, N., et al.: Prediction of conversion from mild cognitive impairment to alzheimer’s disease using mri and structural network features. *Frontiers in Aging Neuroscience* **8**, 76 (2016)
- [45] World Health Organization: Dementia (2023), <https://www.who.int/news-room/fact-sheets/detail/dementia>
- [46] Yeo, B.T.T., Krienen, F.M., Sepulcre, J., et al.: The organization of the human cerebral cortex estimated by intrinsic functional connectivity. *Journal of Neurophysiology* **106**(3), 1125–1165 (2011)
- [47] Yuan, L., Wang, Y., Thompson, P.M., Narayan, V.A., et al.: Multi-source feature learning for joint analysis of incomplete multiple heterogeneous neuroimaging data. *NeuroImage* **61**(3), 622–632 (2012)